Research Square

Preprints are preliminary reports that have not undergone peer review.
They should not be considered conclusive, used to inform clinical practice,
or referenced by the media as validated information.

Cerium oxide nanoparticles conjugated to anti-inflammatory microRNA-146a prevent bleomycin-induced acute lung injury

Stephen Niemiec
University of Colorado
Sarah Hilton
Laboratory for Fetal and Regenerative Biology, Department of Surgery, University of Colorado Denver School of Medicine and Children's Hospital Colorado, Aurora, CO
Alison Wallbank
Department of Bioengineering, University of Colorado, Aurora, CO
Mark Azeltine-Bannerman
Laboratory for Fetal and Regenerative Biology, Department of Surgery, University of Colorado Denver School of Medicine and Children's Hospital Colorado, Aurora, CO
Amanda Louiselle
Laboratory for Fetal and Regenerative Biology, Department of Surgery, University of Colorado Denver School of Medicine and Children's Hospital Colorado, Aurora, CO
Hanan Elajaili
Cardiovascular Pulmonary Research Laboratories and Pediatric Critical Care Medicine, Department of Pediatrics, University of Colorado, Aurora, CO
Ayed Allawzi
Cardiovascular Pulmonary Research Laboratories and Pediatric Critical Care Medicine, Department of Pediatrics, University of Colorado, Aurora, CO
Junwang Xu
Laboratory for Fetal and Regenerative Biology, Department of Surgery, University of Colorado Denver School of Medicine and Children's Hospital Colorado, Aurora, CO
Courtney Mattson
Department of Bioengineering, University of Colorado, Aurora, CO
Lindel Dewberry
Laboratory for Fetal and Regenerative Biology, Department of Surgery, University of Colorado Denver School of Medicine and Children's Hospital Colorado, Aurora, CO
Junyi Hu
Laboratory for Fetal and Regenerative Biology, Department of Surgery, University of Colorado Denver School of Medicine and Children's Hospital Colorado, Aurora, CO
Sushant Singh

Department of Material Science and Engineering, Advanced Materials Processing and Analysis Center, Nanoscience Technology Center, University of Central Florida, Orlando, FL

Tamil Sakthivel

Department of Material Science and Engineering, Advanced Materials Processing and Analysis Center, Nanoscience Technology Center, University of Central Florida, Orlando, FL

Eva Nozik-Grayck

Cardiovascular Pulmonary Research Laboratories and Pediatric Critical Care Medicine, Department of Pediatrics, University of Colorado, Aurora, CO

Bradford Smith

Department of Bioengineering, University of Colorado, Aurora, CO

Sudipta Seal

Department of Material Science and Engineering, Advanced Materials Processing and Analysis Center, Nanoscience Technology Center, University of Central Florida, Orlando, FL

Carlos Zgheib

Laboratory for Fetal and Regenerative Biology, Department of Surgery, University of Colorado Denver School of Medicine and Children's Hospital Colorado, Aurora, CO

Kenneth Liechty (ken.liechty@cuanschutz.edu)

Laboratory for Fetal and Regenerative Biology, Department of Surgery, University of Colorado Denver School of Medicine and Children's Hospital Colorado, Aurora, CO

Research Article

Keywords: Acute lung injury, Acute Respiratory Distress Syndrome, microRNA, nanotechnology

Posted Date: July 7th, 2020

DOI: https://doi.org/10.21203/rs.3.rs-40082/v1

License: This work is licensed under a Creative Commons Attribution 4.0 International License.
Read Full License

Abstract

Acute respiratory distress syndrome (ARDS) is a devastating pulmonary disease with significant inhospital mortality and is the leading cause of death in COVID-19 patients. Potential therapies remain limited despite advancements in understanding ARDS pathophysiology. Excessive leukocyte recruitment, unregulated inflammation, and resultant fibrosis contribute to poor ARDS outcomes. In this study, we evaluated the potential of the radical scavenging cerium oxide nanoparticle (CNP) conjugated to the anti-inflammatory microRNA-146a (CNP-miR146a) to prevent acute lung injury (ALI) following exposure to bleomycin. We have found that CNP-miR146a can prevent ALI by altering leukocyte recruitment, reducing inflammation, and decreasing collagen deposition, ultimately improving pulmonary biomechanics.

Introduction

Acute lung injury (ALI) in its most severe form, acute respiratory distress syndrome (ARDS), is a highly morbid pulmonary disease that carries an in-hospital mortality of nearly 40% worldwide.1,2 The disease accounts for 10% of intensive care unit (ICU) admissions with a median length of ICU stay of 25 days.1,3 The injury seen in ARDS can be secondary to a range of systemic inflammatory insults including trauma, sepsis, and direct lung injury such as through aspiration or toxic exposure.4,5 The burden of this severe disease is rising dramatically due to the novel coronavirus (SARS-CoV–2) causing the disease COVID–19 which escalates to ARDS in approximately 15–40% of patients hospitalized with the disease.6,7 In the United States, this may result in 1,000,000 cases of ARDS in the year 2020 alone.8 ARDS is characterized by hypoxic respiratory failure resultant from diffuse alveolar injury, increased capillary permeability, and surfactant dysfunction,9,10 with long-term sequelae of pulmonary fibrosis and respiratory dysfunction.11,12 Regardless of etiology, excess inflammation and oxidative stress are key components of the progression of ALI to ARDS.

ALI leads to the release of pro-inflammatory mediators from the pulmonary epithelium and endothelium, with alveolar macrophages playing a critical role in the propagation of these inflammatory signals.13 These chemokines promote leukocyte recruitment to the site of injury, particularly neutrophils and, in turn, macrophages. Increased macrophage infiltrate has been associated with activation of the NFκB (nuclear factor kappa-light-chain-enhancer of activated B cells) pathway and upregulation of the target pro-inflammatory cytokines IL–6, IL–8, and TNFα.14,15 Upregulation of pro-inflammatory mediators promotes the release of reactive oxygen species (ROS) and collagen synthesis.16,17

Despite advancements in understanding the pathophysiology of ARDS, therapeutic options targeting the inflammatory response while restoring pulmonary function are limited.18 For example, the anti-inflammatory properties of corticosteroids are well established; however studies evaluating their mortality benefit and improvement in pulmonary function after ALI have had inconsistent conclusions, with results ranging from worsened outcomes to mild improvements.18,19 There is a need for novel therapeutics that will protect the lung from an ongoing inflammatory insult while preventing pulmonary dysfunction and microRNAs (miRNA, miR) are one potential target within these inflammatory pathways.20 miRNAs are

short, noncoding RNA molecules known to modulate gene expression through alteration of messenger RNA (mRNA) translation or promotion of mRNA degradation.21 miR–146a, a key regulator in the inflammatory response with significant anti-inflammatory actions, normally represses tumor necrosis factor receptor-associated factor 6 (TRAF6) and interleukin–1 receptor-associated kinase 1 (IRAK1), activators of the NFκB pathway, ultimately resulting in decreased expression of pro-inflammatory mediators IL–6, IL–8, and TNFα.22 miR–146a has been shown to be upregulated as a defensive response to acute lung injury,23 and overexpression of miR–146a has been shown to suppress pro-inflammatory mediators and to promote a pro-resolving macrophage phenotype in murine models of ALI.24

miRNAs have rapid pharmacokinetics given their small size and negative charge, and are degraded by ubiquitous tissue nucleases, resulting in overall instability as an unmodified therapeutic.25,26 Given the fragile nature of these small nucleotides, development of stable miRNA delivery mechanisms is of growing interest. While therapeutic application of strategies like chemical modification27,28 and viral delivery29 may be limited by bioavailability30,31 or an individual's innate immunity to a virus,32 respectively, nanoparticle technology offers a potential solution, protecting the miRNA from nuclease degradation while stabilizing the nucleotide for cellular uptake.26,28 One such nanoparticle, the cerium oxide nanoparticle (CNP), provides an advantageous delivery mechanism because CNP with multivalent oxidation states (+3, +4) has radical scavenging properties33–39 and may protect the miRNA from oxidative damage while neutralizing its negative charge to promote cellular uptake.40–43 We have previously shown in diabetic wounds that local delivery of miR–146a conjugated to CNP, termed CNP-miR146a, reduces the inflammatory response and accelerates wound healing.44 The suppression of acute inflammation in lung injury could improve pulmonary function and decrease risk of chronic pulmonary disease.

A well-established murine model of ALI/ARDS is toxic exposure to bleomycin that results in a significant inflammatory response, as seen in ARDS, that progresses to fibrosis. We hypothesize that intratracheal administration of CNP-miR146a after bleomycin-induced acute lung injury reduces the inflammatory infiltrate, decreases pro-inflammatory cytokine levels, and lowers oxidative stress, thereby preventing alveolar damage and improving pulmonary function.

Results

Inflammatory Cell Infiltrate

Histologic evidence of inflammatory cells infiltration was evaluated using CD45+ staining in lung tissue harvested 14 days following bleomycin injury (Figure 1A-E). Bleomycin-injured mice demonstrated significantly higher CD45+ cells per high-powered field (HPF) compared to controls ($p = 0.0008$; 95% CI: [83.9, 349.1]).

Preventative treatment with CNP-miR146a significantly decreased the number of CD45+ cells present (Figure 1F, p = 0.0176; 95% CI: [23.03, 288.4]).

ROS Production

The concentration of CM• following oxidation of 1-hydroxy–3-methoxycarbonyl–2, 2, 5, 5-tetramethylpyrrolidine (CMH), a superoxide selective nitroxide probe, was measured in lungs harvested at 14 days following injury using electron paramagnetic resonance (EPR) spectrometry. Bleomycin-injured lungs had higher nitroxide concentrations of 169μM than control concentrations of 126μM (p = 0.0239, 95% CI: [–82.05, - 4.161]). All treatment groups had lower nitroxide concentrations than bleomycin-injured lungs as depicted in Figure 2 (p < 0.0001, F = 11.12, R2 = 0.5596).

Pro-Inflammatory Gene Expression

To evaluate the effects of CNP-miR146a on pro-inflammatory gene expression, real-time quantitative polymerase chain reaction (RT-qPCR) was performed on right lung digests. miR–146a gene expression was evaluated and compared to baseline levels at 4 hours, 3 days and 7 days after injury and with CNP-miR146a prevention treatment at the time of injury. Preventative treatment with CNP-miR146a significantly increased the level of miR–146a 7 days following injury compared to untreated, bleomycin-injured lungs (Figure 3, p = 0.0191, 95% CI: [0.1017, 0.9409]). Preventative treatment had trends toward increasing miR146a expression levels at 4 hours and 3 days following injury.

Figure 4 depicts the relative gene expression of IL–6, IL–8, and TNFα at 3- and 7-days post injury.

Three days after injury, there was a significant increase in IL–6 and TNFα gene expression (p = 0.0025, 95% CI: [2.601, 10.84]; p = 0.0474, 95% CI: [0.02014, 3.512]), with a trend toward an increase in IL–8 in bleomycin- injured mice compared to uninjured controls (p = 0.0867, 95% CI: [–0.29, 4.658]). Preventative treatment with CNP-miR146a significantly lowered IL–6 gene expression compared to untreated, bleomycin-injured mice 3 days following injury (p = 0.0386, 95% CI: [–8.462, –0.2253]). Seven days after bleomycin injury, there was a significant upregulation in IL–6 and IL–8 compared to controls (p < 0.0001, 95% CI: [2.96, 8.668]; p = 0.0002, 95% CI: [1.244, 4.824]). CNP-miR146a treatment lowered expression of IL–8 and TNFα compared to untreated, injured lungs (p = 0.0297, 95% CI: [–3.312, –0.1221]; p = 0.0124, 95% CI: [–2.384, –0.2115]). To test the individual components of the conjugate treatment, CNP-miR146a, treatment with equivalent doses of miR- 146a mimic and CNP alone was performed. miR–146a mimic treatment additionally lowered IL–8 and TNFα gene expression compared to bleomycin-injured lungs that did not receive treatment (p = 0.0495, 95% CI: [- 3.361, –0.0024]; p = 0.0339, 95% CI: [–2.234, –0.0615]). Two weeks following bleomycin injury, expression of IL–6, IL–8, and TNFα returned to control levels in bleomycin-injured lungs with no difference between treated and untreated groups (data not shown).

Pulmonary Fibrosis and Lung Histology

Histologic evaluation of inflation-fixed lung tissue was performed on tissue harvested 14 days following injury to assess overall architectural change and the degree of fibrosis. 4μm sections were trichrome stained and lung injury severity score was evaluated. Bleomycin-injured mice had significantly worse cellular infiltration and cellular hyperplasia when compared to PBS controls ($p = 0.045$, 95% CI: [0.07524, 4.925]), as depicted in Figure 5, with no statistically significant difference in cellular infiltration or cellular hyperplasia between mice treated with CNP-miR146a and control mice. Overall lung injury severity scores had a mean of 1 for controls, 11.5 for bleomycin-injured mice, and 6.5 for prevention-treated mice, although severity scores were not significantly different between the groups ($p = .118$, $F = 3.386$, $R2 = 0.5752$).

Using trichrome-stained slides, collagen deposition was quantified per hpf for each treatment group 14 days following bleomycin injury using NIS-Elements—Advanced Research computer software. There was a significant reduction in area of collagen per hpf with miR146a mimic treatment ($p = 0.0295$, 95% CI: [–20,420, - 775.3]) and with CNP-miR146a treatment ($p = 0.0458$, 95% CI: [–19,777, –132.4]) compared to bleomycin- injured mice (Figure 5). Col1α2 and Col3α1 relative gene expression was evaluated using RT-qPCR. Col1α2 was upregulated 7 days after injury in bleomycin-injured lungs compared to controls ($p = 0.0009$, 95% CI: [0.2382, 1.054]), with gene expression significantly lower in CNP-treated and miR146a-treated lungs compared to untreated, bleomycin-injured lungs ($p < 0.0001$, 95% CI: [–1.226, –0.4408]; $p < 0.0001$, 95% CI: [–1.217, - 0.4321]). There was no significant difference in Col1α2 gene expression among groups at 14 days following injury or in Col3α1 at 7 or 14 days after injury.

Pulmonary Function

Pulmonary function was measured during invasive mechanical ventilation 14 days after bleomycin injury (Figure 6). Quasi-static pressure-volume loop analysis shows that, compared to uninjured controls, the bleomycin-injured mice had significantly lower compliance at 5 cmH20 on the expiratory limb ($p < 0.0001$, 95% CI: [–0.03787, –0.01721]) and decreased inspiratory capacity ($p < 0.0001$, 95% CI: [–0.303, –0.942], while hysteresis was not significantly changed. Multi-frequency forced oscillation impedance measurements recorded at PEEP = 0 cmH2O and fit to the constant phase model show that bleomycin increased pulmonary system elastance ($p = 0.0005$, 95% CI: [7.619, 35.30]) and tissue resistance ($p = 0.0003$, 95% CI: [1.186, 5.507]) while central airway resistance was unaffected. Preventative treatment with CNP-miR146a restored pulmonary compliance, elastance, tissue resistance, and inspiratory capacity to control levels. When compared to untreated, bleomycin-injured lung, CNP-miR146a treatment significantly improved compliance ($p = 0.0107$, 95% CI: [0.00222, 0.0229]), inspiratory capacity ($p = 0.018$, 95% CI: [0.0154, 0.228]), elastance ($p = 0.0324$, 95% CI: [–27.99, –0.869]), and tissue resistance ($p = 0.0362$, 95% CI: [–3.868,––0.0967]).

Discussion

Despite advances in mechanical ventilation and critical care, the progression of acute lung injury to ARDS results in devastating morbidity and an in-hospital mortality of nearly 40%.1 Mortality in patients with COVID–19 who develop ARDS carry an in-hospital mortality of 50%, with some reports suggesting a mortality rate greater than 80% in COVID–19 ARDS.45 Therefore, there is a pressing need to develop novel therapeutics that may prevent ALI and protect pulmonary function. In this experiment, we examined the *in vivo* role of CNP- miR146a in preventing ALI at the time of bleomycin-induced lung injury through modulation of the inflammatory cascade.

Bleomycin-induced lung injury results in a robust inflammatory response with increased inflammatory cell recruitment. Recruited leukocytes, identified histologically using CD45+ staining, play a critical role in the development of ALI. Alveolar macrophages, for instance, play a critical role in both the development of ALI and its resolution as it transitions from a pro-inflammatory activation state to a pro-resolving/anti-inflammatory phenotype.46,47 We see a robust infiltration of leukocytes on histologic analysis of lung tissue 14 days following injury, and treatment with CNP-miR146a reduced this leukocyte infiltrate (Figure 1).

Leukocytes play an important role in free radical production, and excess oxidative stress is intrinsic to the pathogenesis of ALI and ARDS. CNP with its variable valency has the potential to scavenge free radicals, which could explain the reduction in CM• concentration with CNP alone and in conjugation with miR146a (Figure 2). miR146a alone additionally decreased ROS concentration, which we believe is secondary to the promotion of the pro-resolving macrophage phenotype through the anti-inflammatory action of miR–146a.

Higher levels of ROS promote the release of pro-inflammatory cytokines,46 so lowering ROS may aid in the resolution of lung injury. We have previously shown that CNP-miR146a targets the NF-κB pro-inflammatory pathway by inhibiting TRAF6 and IRAK1.44 NF-κB is known to promote IL–6, IL–8, and TNFα cytokine production, which play significant roles in the pathogenesis of ALI.14,15 We found that treatment with CNP- miR146a at the time of injury is able to significantly reduce IL–6 gene expression three days following bleomycin injury. Furthermore, treatment with CNP-miR146a reduced IL–8 and TNFα gene expression seven days following injury. Preventing the early increase in IL–6, which is an early acute-phase reactant, may prevent an inflammatory cascade and prevent persistent elevation of IL–8 and TNFα at later timepoints (Figure 4).

The reduction in inflammation at 3 and 7 days with CNP-miR146a correlates with lower oxidative stress (nitroxide concentration) and inflammatory cell infiltrate 14 days after injury. Early reductions in this inflammatory cascade within the lung, specifically with reductions in IL–6, IL–8, and TNFα, may lower chemokine signaling and leukocyte infiltration. Importantly, there is normalization of gene expression to control levels of IL–6, IL–8, and TNFα 14 days following injury in all treatment groups. This may be attributed to a negative feedback loop driven by the anti-inflammatory miR146a.

miR–146a has an intrinsic role in downregulating inflammation in acute lung injury, however, miR–146a gene expression is initially downregulated in bleomycin-injured lungs and does not return to a baseline

level until 3 days following injury (Figure 3). This may suggest that the role of miR146a in the resolution of pulmonary inflammation is promotion of a negative feedback loop intrinsic to lungs after injury. By treating with CNP-miR146a, we were able to increase miR–146a expression earlier and sustain significant increases in the anti-inflammatory feedback 7 days following lung injury. This early promotion of an anti-inflammatory environment may heighten the potential of this negative feedback loop thereby potentiating the ongoing inflammation seen following bleomycin-induced acute lung injury. Furthermore, given a peak expression level of miR146a three days following injury, treatment with CNP-miR146a at this time point may bolster this negative feedback loop, thereby rescuing the lung from an active inflammatory insult. One risk with decreasing inflammation and promoting an anti-inflammatory microenvironment is the development of infection. By reinforcing an innate negative feedback pathway that returns to baseline, perhaps we would avoid this additional risk, an important factor to consider in human application.

Ultimately, the goal of treatment with CNP-miR146a is to improve long-term outcomes following ALI by decreasing fibrosis and improving pulmonary biomechanics. The long-term effects of ALI/ARDS are often driven by lung structural changes, such as interstitial fibrosis. We see that treatment with CNP-miR146a after bleomycin-induced lung injury protects against the inflammatory infiltration and structural changes seen on histology (Figure 5). While we did not find evidence of differences in collagen gene expression, histologic quantification of collagen deposition demonstrated a marked decrease in collagen protein quantities in mice treated with miR146a mimic or CNP-miR146a compared to untreated, bleomycin-injured mice. We believe that the early reduction of inflammatory gene expression results in less pathologic remodeling. This culminates in the critical challenge in ALI/ARDS treatment: improvement in pulmonary function.

The potential of CNP-miR146a in a clinical setting is highlighted by the prevention of pulmonary mechanical dysfunction with CNP-miR146a. While CNP alone and miR146a alone additionally lower ROS and inflammatory signaling, we found the conjugate treatment to be the most effective in improving pulmonary mechanics (Figure 6). Treatment with CNP-miR146a at the time of injury improved pulmonary elastance, inspiratory capacity, pulmonary compliance, and tissue resistance. By lowering inflammatory signaling and collagen deposition, and improving pulmonary histologic structure, CNP-miR146a prevents acute lung injury and protects pulmonary function. This could prevent the need for mechanical ventilation or ICU admission, and prevent the need for long-term pulmonary rehabilitation.

The rising incidence of COVID–19 and ARDS highlights the absence of effective ARDS therapies. In this study, we show that CNP-miR146a, the conjugate of the free radical scavenging cerium oxide nanoparticle and the anti-inflammatory microRNA–146a, is able to prevent bleomycin-induced acute lung injury. By reducing the inflammatory cell infiltrate, and preventing free radical overproduction and a heightened inflammatory response, CNP-miR146a provides a potential therapeutic for ALI to reduce histologic injury and improve pulmonary mechanics.

Online Methods

Animal Bleomycin Model

Eight- to ten-week-old male mice (C57BL/6, strain No. 000642, Jackson Laboratory) were used after allowing the animals to acclimate to our 1600 m altitude for 1 week. Care of the animals was in accordance with the guidelines defined in the NIH Guide for the Care and Use of Laboratory Animals. Animal protocols were approved by the Institutional Animal Care and Use Committee (IACUC) at University of Colorado Denver – Anschutz Medical Campus (License #84-R–0059). Animals were anesthetized with inhaled isoflurane prior to intratracheal administration of bleomycin or an equal volume of phosphate buffered saline. Animals were euthanized with isofluorane at 4 hours or three, seven, or fourteen days after injury. Lung tissue was harvested for immunohistochemistry or tissue homogenization and molecular testing after ventilatory testing. Each measurement was taken from distinct samples.

Treatment of Bleomycin-Induced Lung Injury

Cerium oxide nanoparticles were synthesized and oxidized, as previously described (17, 18).

Conjugation of CNP to miR146a was performed by utilizing the activated form of 1,1-carbonyldiimidazole (CDI) to couple the amino group of miR146a to the CNP hydroxyl group. Bleomycin-injured mice were given 5 units/kg of bleomycin and were divided into four treatment groups with intratracheal administration of: no treatment (Bleo), 1ng CNP alone (Bleo + CNP), 1ng miR146a mimic alone (Bleo + miR146a), or 1ng CNP- miR146a (Bleo + CNP-miR146a) at time of injury, where CNP and miR146a mimic are the component pieces of the conjugate treatment, CNP-miR146a. Control mice were given an equivalent volume of PBS.

Electron Paramagnetic Resonance (EPR) Spectrometry for Reactive Oxygen Species (ROS) Detection

Lung tissue harvested 7 days following injury (n = 5, 10, 7, 7, 11 for control, bleomycin, bleomycin + CNP, bleomycin + miR146a, bleomycin + CNP-miR146a) was homogenized in sucrose buffer in a 1:6 ratio of lung weight to buffer volume (0.25M sucrose, 10mM TRIS-HCl, 1mM EDTA, pH = 7.4). 60µL of lung homogenate for each sample was mixed with 140µL of Krebs-HEPES buffer (KHB) consisting of 100µM DTPA and 0.2mM CMH. A blank sample of 200µL KHB was used for background signal subtraction. The samples were incubated for 1 hour at 37oC and 150µL samples were loaded in PTFE tubing with rubber seal stoppers.48 ROS production was measured by EPR spectrometry using the superoxide selective spin probe 1-hydroxy–3- methoxycarbonyl–2, 2, 5, 5-tetramethylpyrrolidine (CMH). The Bruker EMX nano X-band spectrometer was used at 77 K with Bruker liquid nitrogen Finger Dewar to detect ROS as CM•. EPR acquisition parameters were: microwave frequency = 9.65 GHz; center field = 3438 G; modulation amplitude = 4.0 G; sweep width = 150 G; microwave power = 0.316 mW; total number of scans = 10;

sweep time = 60 s; and time constant = 1.28 ms. CM• nitroxide radical concentration was obtained by double integration followed by Spin count (Bruker).

Quantitative Real-time PCR (RT-qPCR)

Lung tissue used for RT-PCR was collected 4 hours, 3 days, 7 days, and 14 days following bleomycin-induced lung injury (n = 7 for all treatment groups, n = 14 at 7 days for the Bleo group). Harvested lung tissue was homogenized and total RNA was extracted using TRIzol solution per manufacture instructions (Thermo Fisher Scientific). Resuspended RNA was treated with DNAse I (Thermo Fischer Scientific). 5ng RNA was used for reverse transcriptase amplification for miRNA and 1ng RNA was used for reverse transcriptase amplification for mRNA. RT-qPCR was performed with the BioRad CFX–9600 thermal cycler. Normalization was attained using the housekeeper genes GAPDH for mRNA and U6 for miRNA. Expression analysis of miR146a, TNFα, IL–6, and IL–8 was performed. All samples were examined in triplicate and the average of each triplicate was used for statistical analysis of each sample.

Immunohistochemistry

Lung tissue was harvested at time of euthanasia 14 days after injury. The left lung was inflated with melted agarose solution with care to not overinflate the lung. Once inflated, the lung was removed and placed in 4% Paraformaldehyde (PFA) in 10mL sterile PBS incubated on ice. The lung was kept in PFA at room temperature for 24 hours, then dehydrated in 70% EtOH, and embedded in paraffin prior to sectioning at 4μm. Slides were stained with Mason's trichrome. Lung injury severity score was calculated using previously established methods (n = 2, 2, 4 for control, bleomycin, bleomycin + CNP-miR146a).49 A score of 0 indicated no injury, 1 indicated mild injury, 2 indicated moderate injury, and 3 indicated severe injury.49 Five 100x total magnification high-power fields were randomly imaged for each sample and collagen deposition was quantified using an automated algorithm on NIS Elements—Advanced Research imaging software and averaged for each sample (n = 7 for all treatment groups).

Slides used for immunohistochemistry were deparaffinized and placed in a citrate buffer (pH 6.0). Biocare Medical's Decloaker was used to retrieve the heat-induced epitope and slides were stained with Leica's Bond Rx instrument. Primary CD45 antibodies at 1:50 solutions (BD Biosciences) were applied to the slides, and the slides were developed with a Vectastain Elite ABC kit (Vector Laboratories). Slides were analyzed for the number of CD45-positive cells per high-power field by evaluating five random high-power fields and averaging counts for each sample (n = 7 for all treatment groups).

Pulmonary Function Testing

Fourteen days after lung injury a cohort of mice were invasively ventilated to measure lung function (n = 12, 8, 6, 5, 11 for control, bleomycin, bleomycin + CNP, bleomycin + miR146a, bleomycin + CNP-miR146a

groups). Mice were anesthetized with 100 mg/kg ketamine, 16 mg/kg xylazine, and 3 mg/kg acepromazine via intraperitoneal (IP) injection. Following tracheostomy with an 18-gauge metal cannula, the mice were ventilated with a computer-controlled rodent ventilator (SCIREQ flexiVent). Respiratory drive was suppressed with 0.8 mg/kg IP pancuronium bromide and the electrocardiogram was used to monitor anesthesia. A baseline ventilation with a tidal volume 10 ml/kg at 200 breaths per minute and PEEP = 3 cmH20 was applied for 10 minutes to allow the mice to stabilize on the ventilator. Recruitment maneuvers (RM) consisting of a 3-sec ramp to 30 cmH2O and a 3-sec breath hold were applied a 2-minute intervals during the stabilization period.

Lung function assessments included an RM followed immediately by a stepwise 16-sec pressure-volume (PV) loop with a maximum pressure of 30 cmH2O. The PV loop data were used to calculate the quasi-static compliance at 5 cmH2O on the expiratory limb, PV loop hysteresis area, and the delivered volume which we refer to as the inspiratory capacity. In addition, an RM was applied and immediately followed by four 3-sec multi-frequency forced oscillations (3 ml/kg, 13 mutually prime frequencies from 1 to 20.5 Hz) at 10-sec intervals to measure pulmonary system impedance. The impedance data was fit to the constant phase model50 to determine elastance, tissue damping, and central airway resistance.

Statistical Analyses

Comparison of quantitative data between multiple treatment groups was performed using one-way ANOVA with a two-sided level of significance $\alpha = 0.05$. The mean of each treatment group was compared to the means of the control and bleomycin treatment groups.

Declarations

Author Contributions: All authors listed made substantial contributions to the design, acquisition, analysis, or interpretation of the work presented in this manuscript. Authors have approved the submitted version of the work.

Competing Interest Statement: This work was supported by a Gates Center Grubstake Award. The authors declare financial interest in Ceria Therapeutics.

References

1. Bellani, G., et al. Epidemiology, Patterns of Care, and Mortality for Patients With Acute Respiratory Distress Syndrome in Intensive Care Units in 50 Countries. JAMA 315, 788–800 (2016).
2. Matthay, M. A., et al. Acute respiratory distress syndrome. Nat Rev Dis Primers 5, 18 (2019).
3. Cheung, A.M., et al. Two-year outcomes, health care use, and costs of survivors of acute respiratory distress syndrome. Am J Respir Crit Care Med 174, 538–544 (2006).

4. Kaku, S., et al. Acute Respiratory Distress Syndrome: Etiology, Pathogenesis, and Summary on Management. J Intensive Care Med, 885066619855021 (2019).
5. Pepe, P. E., Potkin, R. T., Reus, D. H., Hudson, L. D. & Carrico, C. J. Clinical predictors of the adult respiratory distress syndrome. Am J Surg 144, 124–130 (1982).
6. Wang, D., et al. Clinical Characteristics of 138 Hospitalized Patients With 2019 Novel Coronavirus-Infected Pneumonia in Wuhan, China. JAMA (2020).
7. Wu, C., et al. Risk Factors Associated With Acute Respiratory Distress Syndrome and Death in Patients With Coronavirus Disease 2019 Pneumonia in Wuhan, China. JAMA Intern Med (2020).
8. Fink, S. Worst-case estimates for U.S. coronavirus deaths. Vol. 2020 (2020).
9. Katzenstein, A. L., Bloor, C. M. & Leibow, A. A. Diffuse alveolar damage—the role of oxygen, shock, and related factors. A review. Am J Pathol 85, 209–228 (1976).
10. Piantadosi, C. A. & Schwartz, D. A. The acute respiratory distress syndrome. Ann Intern Med 141, 460-470 (2004).
11. DiSilvio, B., et al. Complications and Outcomes of Acute Respiratory Distress Syndrome. Crit Care Nurs Q 42, 349–361 (2019).
12. Pierrakos, C., Karanikolas, M., Scolletta, S., Karamouzos, V. & Velissaris, D. Acute respiratory distress syndrome: pathophysiology and therapeutic options. J Clin Med Res 4, 7–16 (2012).
13. Schwartz, M. D., et al. Nuclear factor-kappa B is activated in alveolar macrophages from patients with acute respiratory distress syndrome. Crit Care Med 24, 1285–1292 (1996).
14. Crimi, E. & Slutsky, A. S. Inflammation and the acute respiratory distress syndrome. Best Pract Res Clin Anaesthesiol 18, 477–492 (2004).
15. Kawano, T., et al. Effect of granulocyte depletion in a ventilated surfactant-depleted lung. J Appl Physiol (1985) 62, 27–33 (1987).
16. Cho, H. Y. & Kleeberger, S. R. Mitochondrial biology in airway pathogenesis and the role of NRF2. Arch Pharm Res (2019).
17. Guzel, A., et al. Attenuation of bleomycin induced lung fibrosis by erdosteine and inhibition of the inducible nitric oxide synthase. Bratisl Lek Listy 116, 196–202 (2015).
18. Lewis, S. R., Pritchard, M. W., Thomas, C. M. & Smith, A. F. Pharmacological agents for adults with acute respiratory distress syndrome. Cochrane Database Syst Rev 7, CD004477 (2019).
19. Steinberg, K. P., et al. Efficacy and safety of corticosteroids for persistent acute respiratory distress syndrome. N Engl J Med 354, 1671–1684 (2006).
20. Rajasekaran, S., Pattarayan, D., Rajaguru, P., Sudhakar Gandhi, P. S. & Thimmulappa, R. K. MicroRNA Regulation of Acute Lung Injury and Acute Respiratory Distress Syndrome. J Cell Physiol 231, 2097-2106 (2016).
21. Bartel, D. P. MicroRNAs: genomics, biogenesis, mechanism, and function. Cell 116, 281–297 (2004).
22. Taganov, K. D., Boldin, M. P., Chang, K. J. & Baltimore, D. NF-kappaB-dependent induction of microRNA miR–146, an inhibitor targeted to signaling proteins of innate immune responses. Proc

Natl Acad Sci U S A 103, 12481–12486 (2006).

23. Zeng, Z., et al. Upregulation of miR–146a contributes to the suppression of inflammatory responses in LPS-induced acute lung injury. Exp Lung Res 39, 275–282 (2013).
24. Vergadi, E., et al. Akt2 deficiency protects from acute lung injury via alternative macrophage activation and miR–146a induction in mice. J Immunol 192, 394–406 (2014).
25. Dowdy, S. F. Overcoming cellular barriers for RNA therapeutics. Nat Biotechnol 35, 222–229 (2017).
26. Johannes, L. & Lucchino, M. Current Challenges in Delivery and Cytosolic Translocation of Therapeutic RNAs. Nucleic Acid Ther 28, 178–193 (2018).
27. Bennett, C. F. & Swayze, E. E. RNA targeting therapeutics: molecular mechanisms of antisense oligonucleotides as a therapeutic platform. Annu Rev Pharmacol Toxicol 50, 259–293 (2010).
28. Kaczmarek, J. C., Kowalski, P. S. & Anderson, D. G. Advances in the delivery of RNA therapeutics: from concept to clinical reality. Genome Med 9, 60 (2017).
29. Yin, H., Kauffman, K. J. & Anderson, D. G. Delivery technologies for genome editing. Nat Rev Drug Discov 16, 387–399 (2017).
30. Crooke, S. T., Wang, S., Vickers, T. A., Shen, W. & Liang, X. H. Cellular uptake and trafficking of antisense oligonucleotides. Nat Biotechnol 35, 230–237 (2017).
31. Komarova, Y. & Malik, A. B. Regulation of endothelial permeability via paracellular and transcellular transport pathways. Annu Rev Physiol 72, 463–493 (2010).
32. Kay, M. A. State-of-the-art gene-based therapies: the road ahead. Nat Rev Genet 12, 316–328 (2011).
33. Chen, J., Patil, S., Seal, S. & McGinnis, J. F. Rare earth nanoparticles prevent retinal degeneration induced by intracellular peroxides. Nat Nanotechnol 1, 142–150 (2006).
34. Dowding, J. M., et al. Cerium oxide nanoparticles protect against Abeta-induced mitochondrial fragmentation and neuronal cell death. Cell Death Differ 21, 1622–1632 (2014).
35. Grulke, E., et al. Nanoceria: factors affecting its pro- and anti-oxidant properties. Environ Sci-Nano 1, 429–444 (2014).
36. Heckert, E. G., Karakoti, A. S., Seal, S. & Self, W. T. The role of cerium redox state in the SOD mimetic activity of nanoceria. Biomaterials 29, 2705–2709 (2008).
37. Korsvik, C., Patil, S., Seal, S. & Self, W. T. Superoxide dismutase mimetic properties exhibited by vacancy engineered ceria nanoparticles. Chem Commun (Camb), 1056–1058 (2007).
38. Pirmohamed, T., et al. Nanoceria exhibit redox state-dependent catalase mimetic activity. Chem Commun (Camb) 46, 2736–2738 (2010).
39. Sack, M., et al. Combination of conventional chemotherapeutics with redox-active cerium oxide nanoparticles—a novel aspect in cancer therapy. Mol Cancer Ther 13, 1740–1749 (2014).
40. Colon, J., et al. Cerium oxide nanoparticles protect gastrointestinal epithelium from radiation-induced damage by reduction of reactive oxygen species and upregulation of superoxide dismutase 2. Nanomedicine 6, 698–705 (2010).

41. Hirst, S. M., et al. Anti-inflammatory properties of cerium oxide nanoparticles. Small 5, 2848–2856 (2009).
42. Karakoti, A., Singh, S., Dowding, J. M., Seal, S. & Self, W. T. Redox-active radical scavenging nanomaterials. Chem Soc Rev 39, 4422–4432 (2010).
43. Walkey, C., et al. Catalytic Properties and Biomedical Applications of Cerium Oxide Nanoparticles.*Environ Sci Nano 2,* 33–53 (2015).
44. Zgheib, C., et al. Use of Cerium Oxide Nanoparticles Conjugated with MicroRNA–146a to Correct the Diabetic Wound Healing Impairment. J Am Coll Surg 228, 107–115 (2019).
45. Yang, X., et al. Clinical course and outcomes of critically ill patients with SARS-CoV–2 pneumonia in Wuhan, China: a single-centered, retrospective, observational study. Lancet Respir Med (2020).
46. Fan, E. K. Y. & Fan, J. Regulation of alveolar macrophage death in acute lung inflammation. Respir Res *19,* 50 (2018).
47. Tang, L., et al. M2A and M2C Macrophage Subsets Ameliorate Inflammation and Fibroproliferation in Acute Lung Injury Through Interleukin 10 Pathway. Shock 48, 119–129 (2017).
48. Elajaili, H. B., Hernandez-Lagunas, L., Ranguelova, K., Dikalov, S. & Nozik-Grayck, E. Use of Electron Paramagnetic Resonance in Biological Samples at Ambient Temperature and 77 K. J Vis Exp (2019).
49. Hirano, Y., et al. Neutralization of osteopontin attenuates neutrophil migration in sepsis-induced acute lung injury. Crit Care 19, 53 (2015).
50. Hantos, Z., Daroczy, B., Suki, B., Nagy, S. & Fredberg, J. J. Input impedance and peripheral inhomogeneity of dog lungs. J Appl Physiol (1985) 72, 168–178 (1992).

Figures

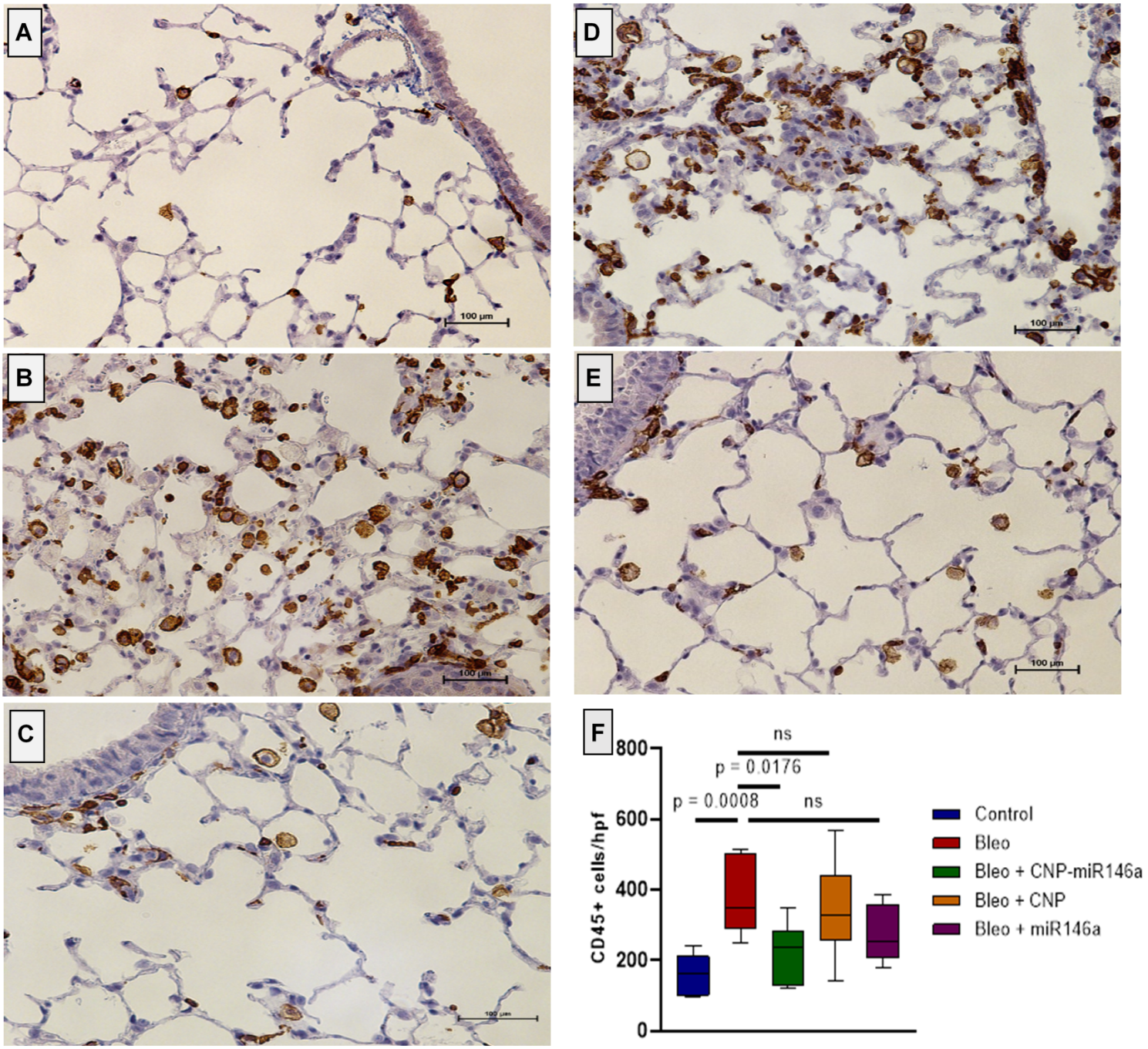

Figure 1

Reduction of inflammatory cell infiltrate with CNP-miR146a. (A-E) CD45+ stained 4µm slides at 200x power 14 days following bleomycin instillation. Acute lung injury with bleomycin resulted in a significant recruitment of leukocytes to pulmonary tissue. (A) Control, (B) Bleomycin, (C) Bleomycin + CNP-miR146a, (D) Bleomycin + CNP, (E) Bleomycin + miR146a. (F) CD45+ cells present in lung samples were significantly higher in bleomycin-injured lungs, and treatment with CNP-miR146a significantly reduced inflammatory cell infiltrate number. Mean and standard deviation values from n = 7 samples per group are shown.

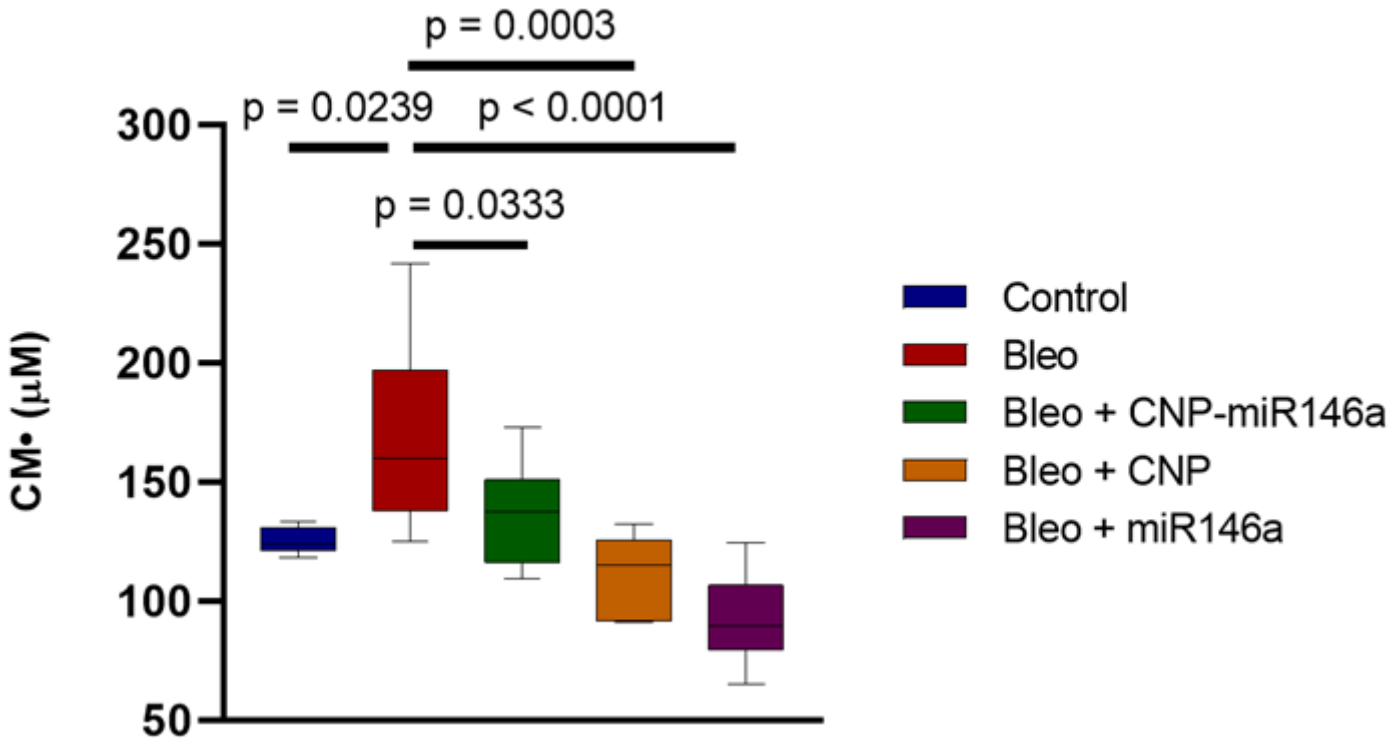

Figure 2

ROS levels 14 days following bleomycin injury measured by EPR. CM• nitroxide reactive oxygen species concentration was significantly higher in bleomycin-injured lungs compared to controls (p = 0.0239), with all treatments normalizing nitroxide concentration to control levels, and reduced to significantly lower levels when compared to untreated bleomycin-injured lungs (p < 0.05). Mean and standard deviation values are shown from n = 5, 10, 11, 7, 7 for control, bleomycin, bleomycin + CNPmiR146a, bleomycin + CNP, bleomycin + miR146a samples per group.

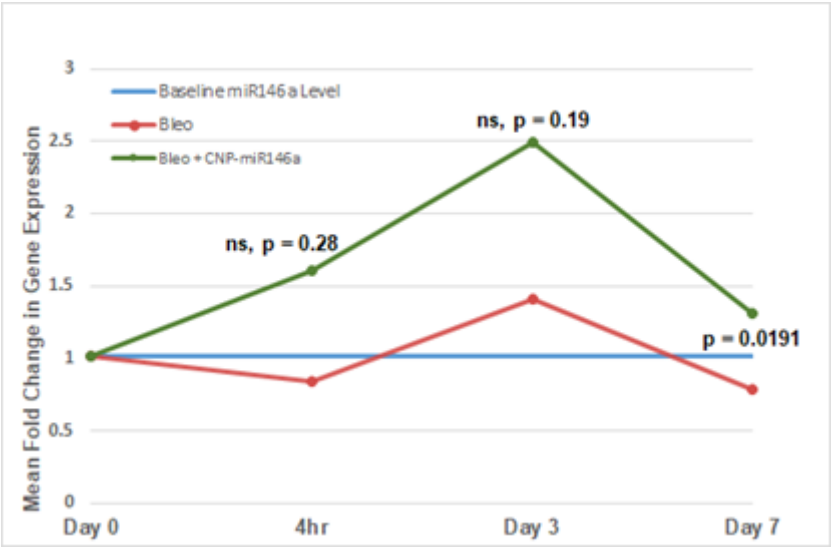

Figure 3

miRNA-146a relative gene expression compared to U6 gene expression. miR146a has decreased initial expression in bleomycin-injured lungs compared to baseline, returning to control levels at day 3. CNP-miR146a treatment significantly increased expression levels of miR-146a at day 7 ($p = 0.0191$). Mean values for n = 5-7 samples per group are shown.

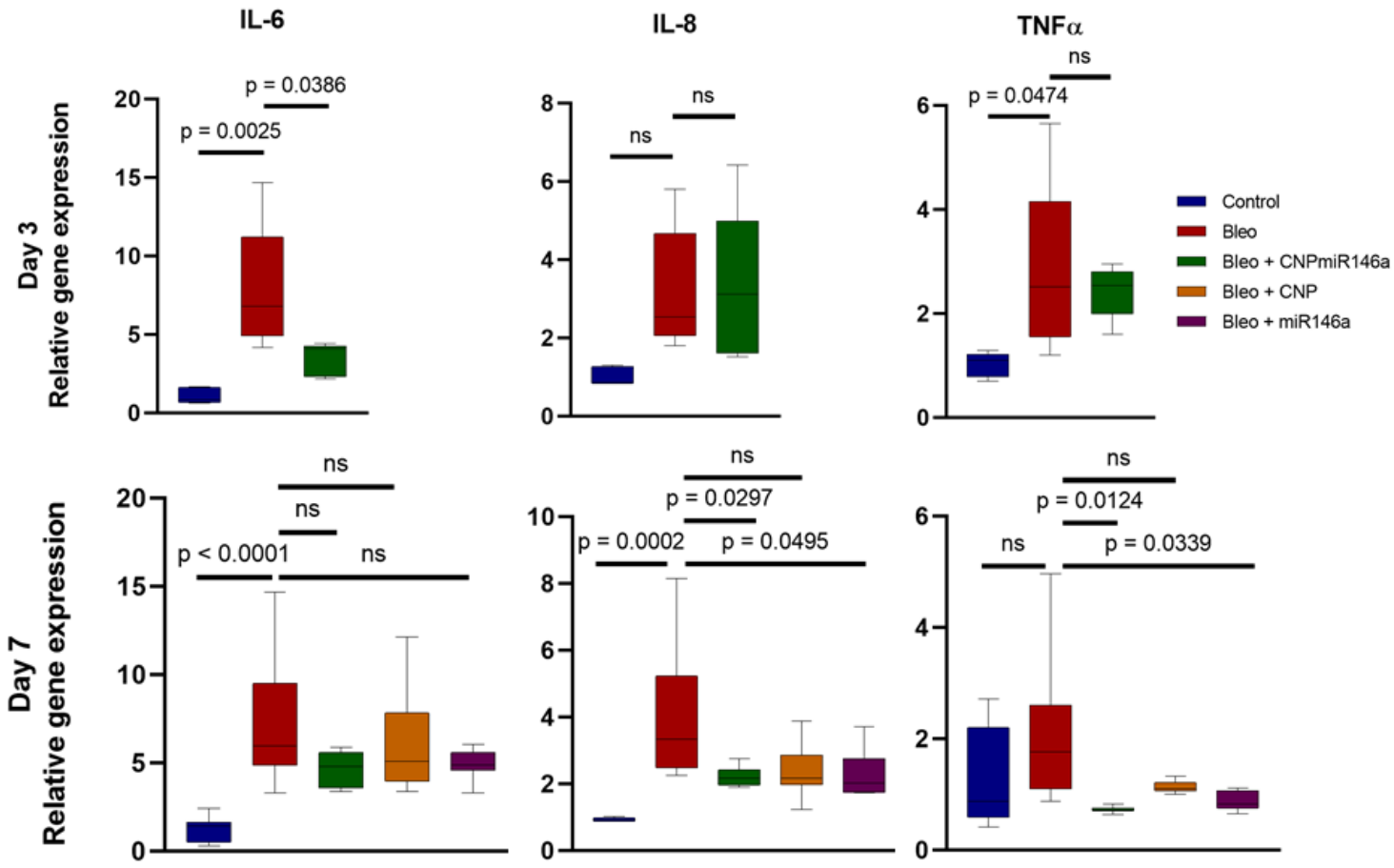

Figure 4

Relative gene expression of pro-inflammatory markers 3- and 7-days after bleomycin injury with comparison to GAPDH housekeeping gene expression. Bleomycin injury significantly raised IL-6, IL-8, and TNFα gene expression compared to controls. IL-6 relative gene expression was significantly reduced with CNP-miR146a 3 days following injury ($p = 0.0386$), while IL-8 and TNFα gene expression were significantly lowered with CNP-miR146a treatment 7 days following injury ($p = 0.0297$ and $p = 0.0124$, respectively). miR146a mimetic also lowered IL-8 and TNFα gene expression 7 days following injury ($p = 0.0495$ and $p = 0.0339$, respectively). Mean and standard deviation for n=7 samples is shown.

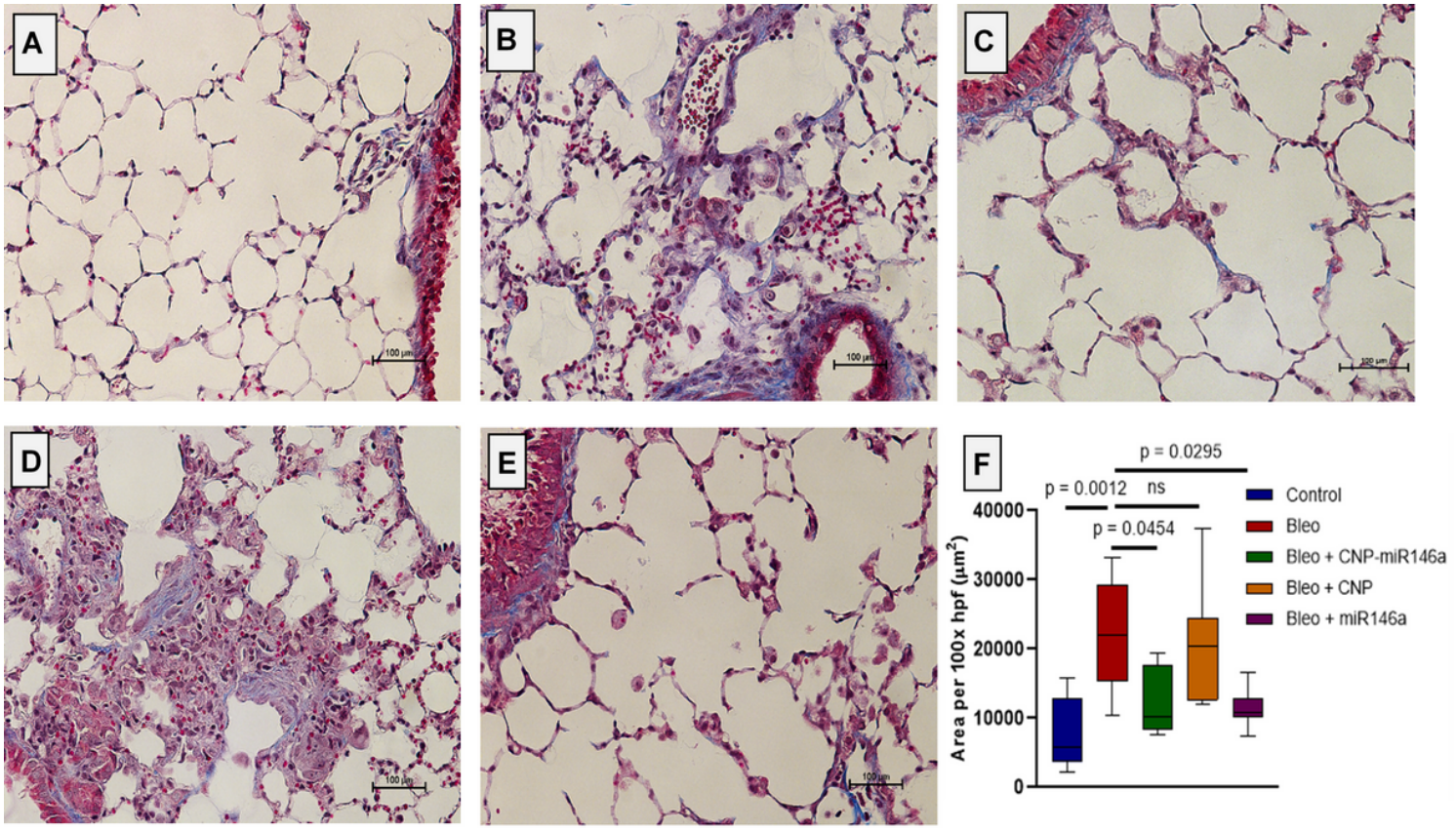

Figure 5

Collagen levels 14 days after bleomycin injury are decreased following CNP-miR146a treatment. Trichrome staining at 200x power (A) control, (B) Bleomycin, (C) Bleomycin + CNP-miR146a, (D) Bleomycin + CNP, and (E) Bleomycin + miR146a lungs. (F) Trichrome quantification of collagen deposition averaged over 5 random high-powered fields (HPF) at 100x power. Bleomycin injury resulted in altered histologic structure and increased collagen deposition in bleomycin-injured lungs compared to controls ($p = 0.0012$). CNP-miR146a treatment and miR146a treatment significantly reduced collagen deposition per HPF compared to bleomycin- injured lungs ($p = 0.0454$, 0.0295 respectively). Mean and standard deviation for $n = 7$ samples are shown.

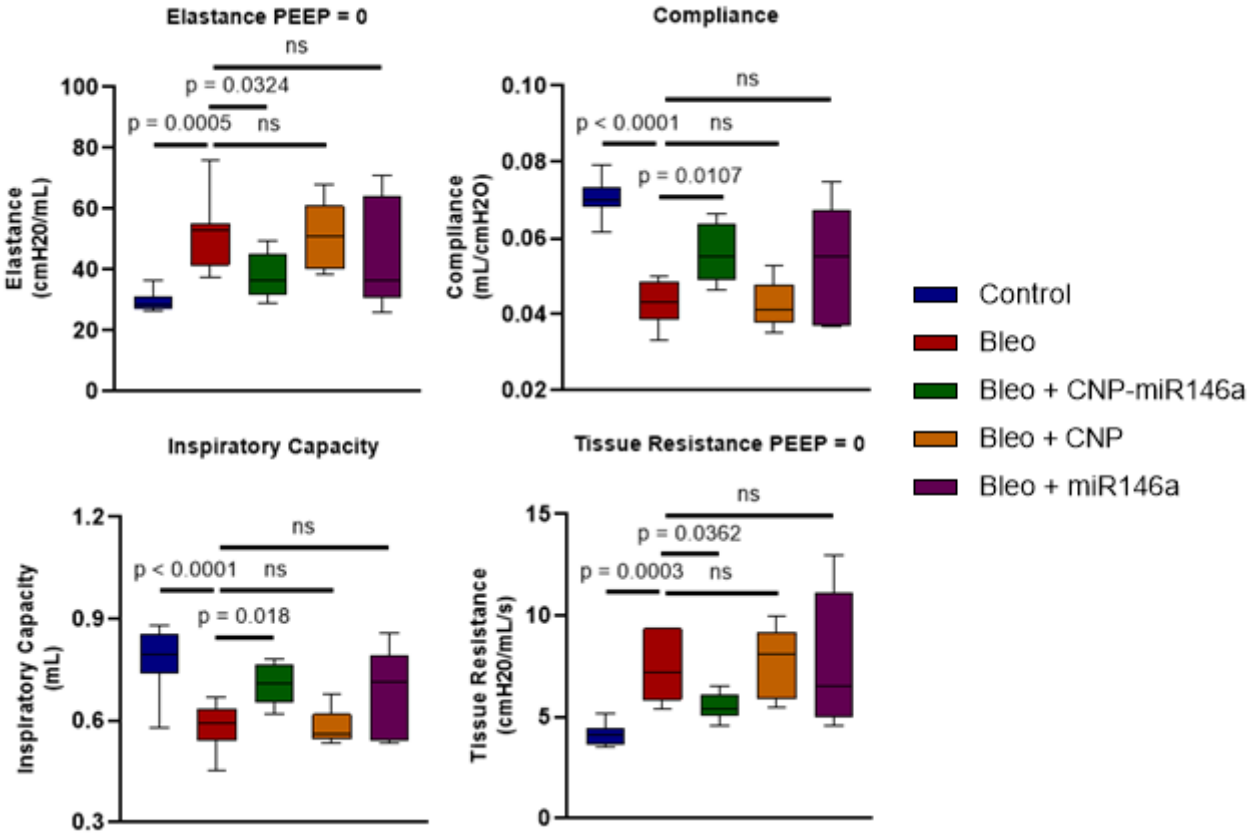

Figure 6

Pulmonary mechanics 14 days after bleomycin injury. Bleomycin-injured mice had significantly worse pulmonary compliance, tissue resistance, elastance, and inspiratory capacity compared to controls, while prevention treatment with CNP-miR146a improved pulmonary mechanics compared to untreated, bleomycin-injured lungs and returned function to control levels. *Control v. experimental group, $p < 0.05$. **Bleomycin v. Treatment group, $p < 0.05$. Mean and standard deviation for n = 12, 8, 6, 5, 11 for control, bleomycin, bleomycin + CNP, bleomycin + miR146a, bleomycin + CNP-miR146a samples are shown.